2,5-Dioxido-1,4-benzoquinonediimine (H_2L^{2-}), A Hydrogen-Bonding Noninnocent Bridging Ligand Related to Aminated Topaquinone: Different Oxidation State Distributions in Complexes [{(bpy)$_2$Ru}$_2$(μ-H$_2$L)]^n (n=0,+,2+,3+,4+) and [{(acac)$_2$Ru}$_2$(μ-H$_2$L)]^m (m=2−,−,0,+,2+)

Sanjib Kar,[a] Biprajit Sarkar,[b] Sandeep Ghumaan,[a] Deepa Janardanan,[a] Joris van Slageren,[c] Jan Fiedler,[d] Vedavati G. Puranik,[e] Raghavan B. Sunoj,*[a] Wolfgang Kaim,*[b] and Goutam Kumar Lahiri*[a]

Abstract: The symmetrically dinuclear title compounds were isolated as diamagnetic [(bpy)$_2$Ru(μ-H$_2$L)Ru(bpy)$_2$]-(ClO$_4$)$_2$ (**1**-(ClO$_4$)$_2$) and as paramagnetic [(acac)$_2$Ru(μ-H$_2$L)Ru(acac)$_2$] (**2**) complexes (bpy=2,2′-bipyridine; acac$^−$=acetylacetonate=2,4-pentanedionato; H$_2$L=2,5-dioxido-1,4-benzoquinonediimine). The crystal structure of **2**·2H$_2$O reveals an intricate hydrogen-bonding network: Two symmetry-related molecules **2** are closely connected through two NH(H$_2$L^{2-})···O-(acac$^−$) interactions, while the oxygen atoms of H$_2$L^{2-} of two such pairs are bridged by an (H$_2$O)$_8$ cluster at half-occupancy. The cluster consists of cyclic (H$_2$O)$_6$ arrangements with the remaining two *exo*-H$_2$O molecules connecting two opposite sides of the *cyclo*-(H$_2$O)$_6$ cluster, and oxido oxygen atoms forming hydrogen bonds with the molecules of **2**. Weak antiferromagnetic coupling of the two ruthenium(III) centers in **2** was established by using SQUID magnetometry and EPR spectroscopy. Geometry optimization by means of DFT calculations was carried out for **1**$^{2+}$ and **2** in their singlet and triplet ground states, respectively. The nature of low-energy electronic transitions was explored by using time-dependent DFT methods. Five redox states were reversibly accessible for each of the complexes; all odd-electron intermediates exhibit comproportionation constants $K_c > 10^8$. UV-visible-NIR spectroelectrochemistry and EPR spectroscopy of the electrogenerated paramagnetic intermediates were used to ascertain the oxidation-state distribution. In general, the complexes **1**$^{n+}$ prefer the ruthenium(II) configuration with electron transfer occurring largely at the bridging ligand (μ-H$_2$L^{n-}), as evident from radical-type EPR spectra for **1**$^{3+}$ and **1**$^+$. Higher metal oxidation states (III, IV) appear to be favored by the complexes **2**^{m}; intense long-wavelength absorption bands and Ru^{III}-type EPR signals suggest mixed-valent dimetal configurations of the paramagnetic intermediates **2**$^+$ and **2**$^−$.

Keywords: bridging ligands · density functional calculations · EPR spectroscopy · N,O ligands · ruthenium

[a] S. Kar, S. Ghumaan, D. Janardanan, Prof. Dr. R. B. Sunoj,
Prof. Dr. G. K. Lahiri
Department of Chemistry
Indian Institute of Technology
Bombay, Powai, Mumbai 400076 (India)
Fax: (+91) 022-2572-3480
E-mail: sunoj@chem.iitb.ac.in
          lahiri@chem.iitb.ac.in

[b] B. Sarkar, Prof. Dr. W. Kaim
Institut für Anorganische Chemie
Universität Stuttgart, Pfaffenwaldring 55
70550 Stuttgart (Germany)
Fax: (+49) 711-685-4165
E-mail: kaim@iac.uni-stuttgart.de

[c] Dr. J. van Slageren
1. Physikalisches Institut
Universität Stuttgart, Pfaffenwaldring 57
70550 Stuttgart (Germany)

[d] Dr. J. Fiedler
J. Heyrovský Institute of Physical Chemistry
Academy of Sciences of the Czech Republic
Dolejškova 3, 18223 Prague (Czech Republic)

[e] Dr. V. G. Puranik
Center for Materials Characterization
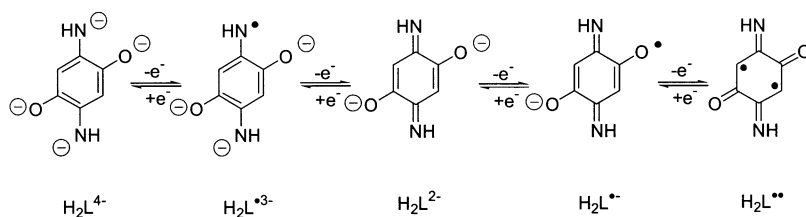National Chemical Laboratory
Pune, Maharashtra 411008 (India)

Supporting information for this article is available on the WWW under http://www.chemeurj.org/ or from the authors.

Introduction

The present work is part of our continuing efforts in designing new classes of ligand-bridged diruthenium complexes that exhibit strong intermetallic electronic coupling in their mixed-valence states through the effective overlap with suitably placed ligand π or π^* orbitals in the bridge.[1] Intramolecular electron transfer between metal ions in polynuclear arrays is of fundamental importance for the design of molecular electronic devices.[2] The extent of metal–metal coupling can be substantially tuned by a judicious selection of ancillary functions.[1]

The recognition of variable electronic delocalization between the frontier π orbitals of quinone derivatives and metal $d\pi$ orbitals in mononuclear systems[3] has initiated programs of exploring quinone-based noninnocent bridging units useful for the construction of polynuclear complexes. In this context, the doubly deprotonated forms of 2,5-dihydroxy-1,4-benzoquinones,[4,5] 5,8-dihydroxy-1,4-naphthoquinone,[6] 1,4-dihydroxyanthraquinone[7] and 1,5-dihydroxyanthraquinone[7] with [O,O;O,O] bis-chelate coordination as well as anions of potentially [N,N;N,N] bis-chelating 2,5-diamino-1,4-benzoquinonediimines[8,9] and 1,2,4,5-tetraimino-3,6-diketocyclohexane[10] have been studied in recent years as bridging ligands in polymetallic complexes containing Ru, Mo, Rh, Ni, Cu, or Pt. However, the analogous doubly deprotonated 2,5-dihydroxy-1,4-benzoquinonediimine bridging ligand, (H_2L^{2-}), with an $[O,N;O,N]^{2-}$ donor set has not yet been explored; an N,N′-disubstituted form was used recently in connection with dinickel(II)-catalyzed olefin polymerization,[11a] and an isomeric system based on 2-hydroxy-5-amino-1,4-benzoquinonemonoimine was described very recently by Braunstein and co-workers.[11b] The present article describes the synthesis of $[\{(bpy)_2Ru^{II}\}_2(\mu\text{-}H_2L^{2-})](ClO_4)_2$ (1-$(ClO_4)_2$) and $[\{(acac)_2Ru^{III}\}_2(\mu\text{-}H_2L^{2-})]$ (2) (bpy = 2,2′-bipyridine, acac$^-$ = acetylacetonate = 2,4-pentanodionato, H_2L = 2,5-dioxido-1,4-benzoquinonediimine), the crystal structure of 2·2H$_2$O, which has an intricate hydrogen-bonding network, and EPR and UV-visible-NIR spectroelectrochemical investigations of the metal–ligand valence combinations in $\mathbf{1}^{n+}$ ($n = 0,1,2,3,4$) and $\mathbf{2}^m$ ($m = 2-,-,0,+,2+$). We address such issues as the efficacy of H_2L^{2-} for metal–metal coupling in various mixed-valent states, particularly with respect to other relevant mediators, the role of the electronic effects from the ancillary ligands, bpy (π-acidic) and acac$^-$ (electron-donating), for the valence-state composition of the complexes as well as their participation in the coupling processes. Whereas the readily accessible metal oxidation states are Ru^{II}, Ru^{III}, and Ru^{IV}, the bridging ligand can adopt an aromatic form H_2L^{4-}, a semiquinone state $H_2L^{\bullet 3-}$, and the quinonoid form H_2L^{2-}. Further oxidation through $H_2L^{\bullet-}$ to a presumed triplet species $H_2L^{\bullet\bullet}$ is considered less favorable because of the high energies and reactivities involved.

1,2,4,5-Donor-substituted benzenes as well as corresponding semiquinone and iminoquinone intermediates are also part of the postulated reaction cycles for copper-dependent amine oxidase enzymes; this may involve electron-transfer interactions between metal and ligand.[12] Considering the hydrogen-bonding network present in corresponding protein structures,[12c–h] it is fortunate that we could obtain the molecules of 2 crystallizing with water clusters (H$_2$O)$_8$, showing intracluster, intermolecule, and cluster–molecule hydrogen-bonding interactions.
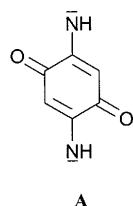
Results and Discussion

Synthesis, identification, and structure: The complexes $[\{(bpy)_2Ru\}_2(\mu\text{-}H_2L)](ClO_4)_2$ (1-$(ClO_4)_2$) and $[\{(acac)_2Ru\}_2(\mu\text{-}H_2L)]$ (2) were prepared by reactions of $[(bpy)_2Ru(EtOH)_2]^{2+}$ or $[(acac)_2Ru(CH_3CN)_2]$, respectively, with 1,4-diamino-2,5-hydroquinone (H$_6$L) in a 2:1 molar ratio in the presence of excess CH$_3$COONa (Scheme 1). During the reaction, the H$_6$L ligand underwent a $2e^-/4H^+$ oxidation pre-
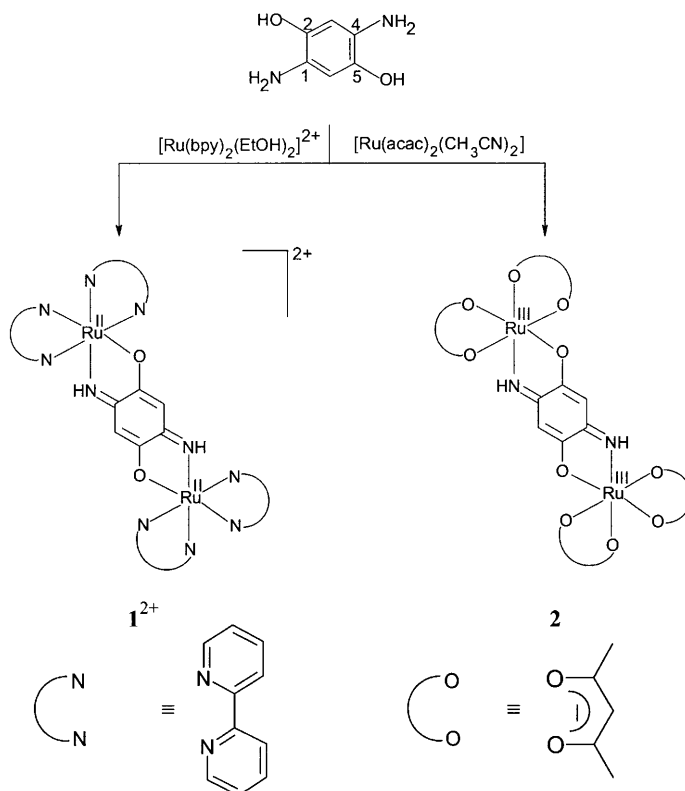
Scheme 1.

sumably by O_2 to the state of 2,5-dioxido-1,4-benzoquinone-diimine (H_2L^{2-}), which symmetrically bridges two units of the metal-complex fragment, either $[Ru^{II}(bpy)_2]^{2+}$ or $[Ru^{III}-(acac)_2]^+$ in 1^{2+} or **2**, respectively, through the anionic O^- and imino nitrogen ($=NH$) donor centers at each end. While the $+2$ oxidation state of the ruthenium ion in the precursor $\{Ru^{II}(bpy)_2\}$ is retained in 1^{2+}, the Ru^{II} state of the starting $\{Ru^{II}(acac)_2\}$ moiety oxidizes to the $+3$ state in **2**. The presence of electron-rich $acac^-$ ancillary ligands in **2** as opposed to the π-acidic bpy in 1^{2+} facilitates the stabilization of the Ru^{III} state in **2**; this is also reflected in the redox potentials (see later).

In principle, H_2L^{2-} could also exist in the alternative benzoquinone (**A**) form; however, the preferential stabilization of the benzoquinonediimine form is supported by the crystal structure of $2\cdot2H_2O$ (see below). The greater electronegativity of oxygen relative to nitrogen favors the diimine structure.

Purity and identity of the complexes is demonstrated by their satisfactory elemental analyses (see Experimental Section) and by the electrospray (ES) mass spectra. The observed ES+ signals are centered at m/z values of 1062.8 and 735.18/637.1 for **1**-$(ClO_4)_2$ and **2**, respectively (Figure S1 in the Supporting Information), which correspond to $[1\text{-}ClO_4]^+$ (calculated mass: 1062.45) and $[2]^+$ (calculated mass: 734.69)/$[2-acac]^+$ (calculated mass: 636.97).

The presence of the *p*-quinonediimine form of H_2L^{2-} in **2** is supported by a single-crystal X-ray structural study of $2\cdot2H_2O$, with **2** in the *meso* configuration (see below; Figure 1). Crystallographically important parameters and selected bond lengths and angles are given in Tables 1 and 2.
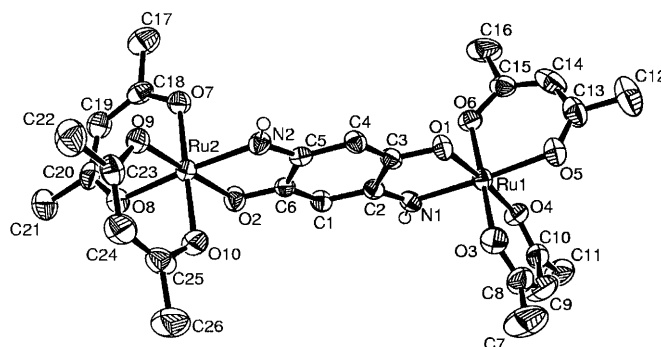

Figure 1. ORTEP diagram of **2**. Ellipsoids are drawn at 50% probability.

average deviation being only 0.2 Å. The intraring bond lengths involving the bridging H_2L^{2-} ligand (Table 2) establish that the C=C double bonds are associated only with the C3—C4 (1.357(9) Å) and C6—C1 bonds (1.353(9) Å). The C2—N1 (1.295(8) Å) and C3—O1 (1.323(7) Å) bonds linked to Ru1 signify double and single bonds, respectively, whereas the corresponding C5—N2 (1.310(8) Å) and C6—O2 (1.314(7) Å) bonds connected with Ru2 exhibit rather similar lengths. The comparison of C—C, C—O, C—N, Ru—O, and Ru—N bond lengths involving H_2L^{2-} in **2** with those of the mononuclear *o*-quinonoid derivatives reported earlier by us[3a] or Bhattacharya and Pierpont[3d] justifies the Ru^{III}(*p*-quinonediimine)Ru^{III} formulation of **2**, as shown in Scheme 1.

The crystal structure analysis of $2\cdot2H_2O$ reveals an intricate hydrogen-bonding network (Figure 2, Table 3). Two symmetry-related molecules of **2** are closely connected through two $NH(H_2L^{2-})\cdots O(acac^-)$ interactions at about 3.02 Å ($O\cdots N$ distance). The other type of anionic oxygen centers in **2**, the $O(H_2L^{2-})$ atoms of two pairs of symmetry-related molecules of **2** are bridged by $(H_2O)_8$ clusters at half-occupancy. Water clusters in crystals of coordination compounds are not uncommon;[13] however, the present case shows quite a remarkable example of not only intermolecular, but also intracluster and cluster–molecule hydrogen bonding (Figure 2). Each cluster consists of a cyclic $(H_2O)_6$ arrangement, and the remaining two *exo*-H_2O molecules (O11) connect two opposite sides of *cyclo*-$(H_2O)_6$ with oxido oxygen atoms (O2) at the molecules of **2**. All O—O lengths are at or below 3.0 Å (Table 3), confirming the stability of the hydrogen-bond network.

Thus, having both basic O^- and, through Ru^{III} coordination, acidic NH functions in the same complex molecule strongly facilitates the tendency towards intramolecular hydrogen bonding as well as towards addition and structuring

Table 1. Crystallographic data for $2\cdot2H_2O$.

formula	$C_{26}H_{36}N_2O_{12}Ru_2$	T [K]	295 [2]K
M_r	770.71	hkl range	$-14 \leq h \leq 14$
crystal size [mm]	$0.35 \times 0.12 \times 0.04$		$-23 \leq k \leq 23$
crystal system	monoclinic		$-17 \leq l \leq 17$
space group	$P2_1/c$	ρ_{calcd} [g cm^{-3}]	1.488
a [Å]	12.185(2)	2θ range [°]	5 to 50
b [Å]	19.871(4)	reflections collected	32245
c [Å]	14.864(3)	unique reflections [R_{int}]	6066 [0.0554]
β [°]	107.044(3)	data/restraints/parameters	6066/0/405
V [Å^3]	3440.9(12)	$R1$ [$I > 2\sigma(I)$]	0.0527
Z	4	$wR2$ [all data]	0.1565
$F(000)$	1560	goodness-of-fit	1.112
μ [mm^{-1}]	0.934	residual electron density [e Å^{-3}]	1.230, -0.387

Note the discrepancy between positional numbering of H_2L^{2-} according to organic nomenclature (Scheme 1) and the numbering of the crystal structure of **2**. The H_2L^{2-} ligand bridges the two Ru^{3+} ions symmetrically in a bis-bidentate fashion through the anionic O^- and imino nitrogen donor centers. The Ru1–Ru2 separation is 7.864 Å; the two ruthenium(III) ions lie in plane with the bridging ligand, the

atoms (O2) at the molecules of **2**. All O—O lengths are at or below 3.0 Å (Table 3), confirming the stability of the hydrogen-bond network.

Table 2. Experimental and calculated selected bond lengths [Å] and angles [°] for **2**.

	Bond lengths			Bond angles	
	Exptl[a]	Calcd[b]		Exptl[a]	Calcd[b]
Ru1−O3	1.993(5)	2.024	O3-Ru1-O4	91.30(18)	88.93
Ru1−O4	2.003(4)	2.031	O3-Ru1-N1	91.90(19)	93.17
Ru1−N1	2.010(5)	2.036	O4-Ru1-N1	96.7(2)	97.37
Ru1−O6	2.012(4)	2.020	O3-Ru1-O6	178.85(19)	179.04
Ru1−O1	2.013(4)	2.028	O4-Ru1-O6	89.73(17)	90.68
Ru1−O5	2.054(5)	2.051	N1-Ru1-O6	87.46(19)	87.75
Ru2−O7	1.999(4)	2.020	O3-Ru1-O1	85.47(19)	88.85
Ru2−O10	2.009(5)	2.025	O4-Ru1-O1	175.02(17)	175.73
Ru2−O2	2.010(4)	2.028	N1-Ru1-O1	79.68(2)	79.12
Ru2−O9	2.009(4)	2.031	O6-Ru1-O1	93.47(17)	91.60
Ru2−N2	2.021(6)	2.036	O3-Ru1-O5	88.1(19)	88.98
Ru2−O8	2.038(5)	2.051	O4-Ru1-O5	89.35(19)	88.63
N1−C2	1.293(8)	1.322	N1-Ru1-O5	173.99(19)	173.66
N2−C5	1.314(8)	1.322	O6-Ru1-O5	92.44(19)	90.13
O1−C3	1.321(7)	1.324	O1-Ru1-O5	94.32(17)	94.98
O2−C6	1.314(7)	1.324	O7-Ru2-O10	178.10(19)	179.04
C1−C6	1.357(9)	1.378	O7-Ru2-O2	91.07(17)	91.60
C1−C2	1.418(8)	1.413	O10-Ru2-O2	87.03(19)	88.84
C2−C3	1.488(8)	1.494	O7-Ru2-O9	90.60(17)	90.68
C3−C4	1.361(9)	1.378	O10-Ru2-O9	91.3(19)	88.93
C4−C5	1.415(9)	1.413	O2-Ru2-O9	176.40(18)	175.72
C5−C6	1.493(8)	1.494	O7-Ru2-N2	87.63(19)	87.75
Ru1−Ru2	7.864	7.958	O10-Ru2-N2	92.20(19)	93.17
			O2-Ru2-N2	80.09(19)	79.12
			O9-Ru2-N2	96.80(19)	97.36
			O7-Ru2-O8	92.54(17)	90.14
			O10-Ru2-O8	87.42(18)	88.98
			O2-Ru2-O8	93.79(18)	94.98
			O9-Ru2-O8	89.31(18)	88.63
			N2-Ru2-O8	173.88(19)	173.67
			O2-C6-C5	116.0(5)	115.98
			N2-C5-C6	113.5(5)	112.91
			O1-C3-C2	115.8(5)	115.97
			N1-C2-C3	113.4(5)	112.91

[a] From X-ray crystal data. [b] Calculated at the B3LYP level of theory by employing the LanL2DZ basis set for Ru and 3-21G for all other atoms.
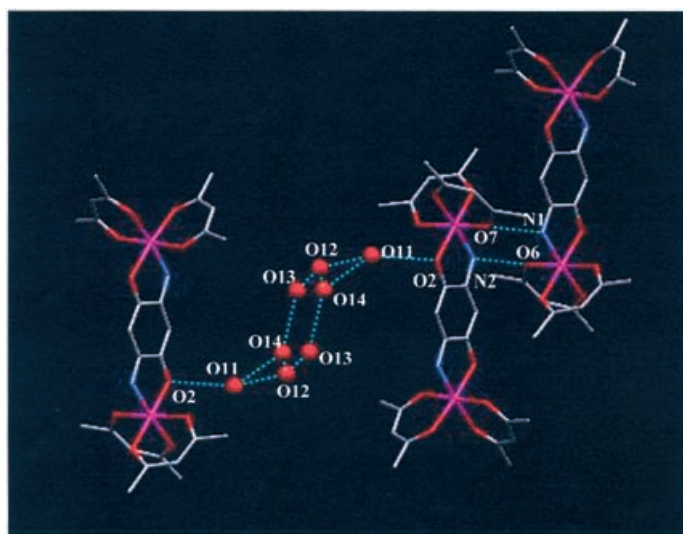

Figure 2. Hydrogen bonding network in **2**·2H$_2$O.

Table 3. Distances relevant to hydrogen bonds in **2**·2H$_2$O.

Atom1	Atom2	Symm1	Symm2	Distance [Å]
O7	N1	x,y,z	$x,0.5-y,-0.5+z$	2.992
N2	O6	x,y,z	$x,0.5-y,-0.5+z$	3.044
O2	O11	x,y,z	$x,0.5-y,-0.5+z$	2.939
O12	O11	x,y,z	$1-x,0.5+y,1.5-z$	2.724
O12	O13	x,y,z	$1-x,1-y,1-z$	2.825
O12	O14	x,y,z	x,y,z	2.930
O13	O12	x,y,z	$1-x,1-y,1-z$	2.825
O13	O14	x,y,z	x,y,z	2.911
O14	O11	x,y,z	$1-x,0.5+y,1.5-z$	3.002
O12	O11	$1-x,1-y,1-z$	$x,0.5-y,-0.5+z$	2.724
O12	O14	$1-x,1-y,1-z$	$1-x,1-y,1-z$	2.930
O14	O11	$1-x,1-y,1-z$	$x,0.5-y,-0.5+z$	3.002
O14	O13	$1-x,1-y,1-z$	$1-x,1-y,1-z$	2.911
O11	O2	$1-x,0.5+y,1.5-z$	$1-x,1-y,1-z$	2.939

of water of crystallization. A detailed study of the influence of such interactions on the electronic properties in protic media will therefore be among the projects resulting from the present investigation, especially since hydrogen-bonding networks are often known to be essential for the control of active-site reactivity in metalloproteins.[12,14]

The computed structural parameters of **2** in its triplet ground state at the B3LYP level of theory are found to be in good agreement with the corresponding values obtained from the X-ray structure (Table 2, Figure 3). The largest de-
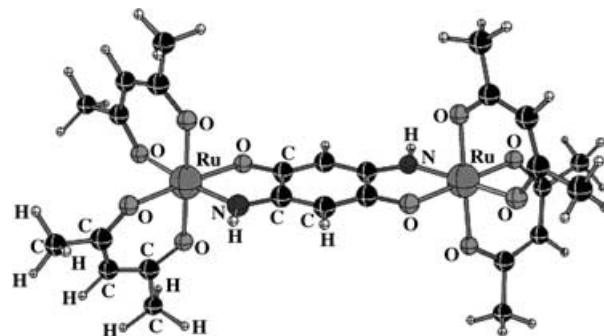

Figure 3. Optimized geometry for the triplet ground-state of **2** at the B3LYP/3-21G level.

viations between experimental and computed bond lengths and angles are only about 0.09 Å and 3.4°, respectively. It should be noted that the agreement between the computed (7.96 Å) and experimental (7.86 Å) intermetallic separation between the Ru^{III} centers is also good.

The optimized geometry for **1**$^{2+}$ in its singlet ground state is summarized in Table S1 and Figure S2 in the Supporting Information. As in the case of **2**, the planarity of the bridging ligand in **1**$^{2+}$ is evident from the optimized geometry. The intermetallic separation between the (larger) ruthenium(II) centers in **1**$^{2+}$ is calculated at 8.075 Å, which is slightly longer than that in **2**.

The dinuclear complexes **1**-(ClO$_4$)$_2$ and **2** with three bidentate ligands around each metal center should be able to exist as pairs of enantiomers (ΔΔ, ΛΛ; C_2 symmetry) or as

the *meso* form (Δ,Λ; C_s symmetry).[15] The ^{1}H NMR spectrum of $\mathbf{1}^{2+}$ clearly exhibits only one set of signals, corresponding to either the *meso* or the *rac* form; an unambiguous identification was not possible. The crystal structure of paramagnetic **2** confirms its *meso* configuration, the other data also support the presence of only one isomer.

The ^{1}H NMR spectrum of **1**-(ClO$_4$)$_2$ in (CD$_3$)$_2$SO shows two clear singlets at $\delta = 5.58$ and 9.67 ppm, corresponding to the CH and NH protons of the bridging ligand. The expected 16 bipyridine proton resonances appear in the region between $\delta = 7.2$ and 8.8 ppm as a partially overlapping cluster of signals (Figure 4).
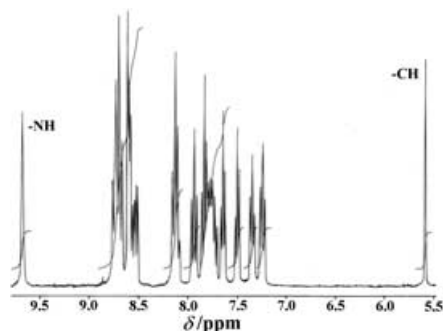
Figure 4. ^{1}H NMR spectrum of **1**-(ClO$_4$)$_2$ in (CD$_3$)$_2$SO.

In agreement with the oxidation state assignment in Scheme 1, compound **2** does not exhibit a well-resolved ^{1}H NMR spectrum, but rather exhibits an EPR signal and magnetic susceptibility that reflect the diruthenium(III) configuration. The EPR spectrum of **2** at 4 K shows a weak but distinct half-field signal at $g = 4.26$ in addition to the axial pattern for d^5 configuration ($g_{1,2} = 2.26$ and $g_3 = 1.81$) (Figure 8a, see later), indicating an accessible triplet state ($S = 1$).[16]

Both complexes **1**-(ClO$_4$)$_2$ and **2** are paramagnetic as evidenced by SQUID magnetometric measurements. For **1**-(ClO$_4$)$_2$ this seems to contradict the $+2$ oxidation state assigned to the ruthenium ions and to the closed-shell character of the bridging ligand. However, the magnetic susceptibility (χ) of **1**-(ClO$_4$)$_2$ is virtually temperature-independent between 300 and 30 K; at lower temperatures it rises proportionally with respect to $1/T$. The latter is probably due to very small amounts of a paramagnetic impurity, while the former can be assigned to temperature-independent paramagnetism (TIP).[16] The TIP phenomenon arises from mixing induced by spin-orbit coupling of the excited-state orbital angular momentum into the ground state. It has been observed before, although usually the absolute value is of the order of $\chi^{TIP} = 10^{-4}$–10^{-3} cm^{3}mol^{-1}, while for **1**-(ClO$_4$)$_2$ $\chi^{TIP} = 0.011$ cm^{3}mol^{-1}.[17] The large χ^{TIP} value leads to a steep slope in the χT versus T plot (Figure 5). A similar, even slightly steeper slope can be observed in the χT curve for **2** from room temperature down to about 50 K. Below that the χT value drops more quickly. This last feature is attributed to weak antiferromagnetic exchange coupling. A fit
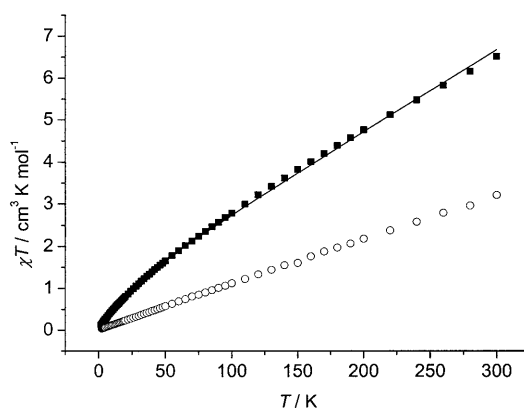

Figure 5. χT versus T recorded on powder samples of **1**-(ClO$_4$)$_2$ (open circles) and **2** (filled squares). The drawn line is a fit to the data for **2**.

using χ^{TIP}, the g value, and the exchange coupling constant ($\mathscr{H} = -2J\mathbf{S}_i\cdot\mathbf{S}_j$) as free parameters yields the following values: $\chi^{TIP} = 0.021 \pm 0.001$ cm^{3}mol^{-1} and $J = -4 \pm 1$ cm^{-1}. The g value is incredibly low at $g = 1.62$, which may be due to the interdependence of the fit parameters. The fit is good at higher temperatures (see Figure 5), whereas the calculated χT value is lower than that calculated at lower temperatures.

Electrochemistry and EPR spectroscopy: In CH$_3$CN, **1**-(ClO$_4$)$_2$ exhibits two successive oxidation couples (Figure 6a, Table 4). The intermediate $\mathbf{1}^{3+}$ displays a very intense band

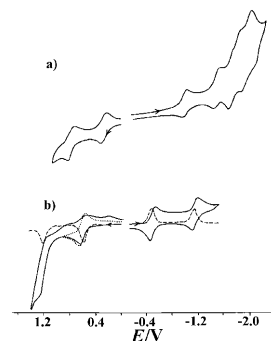Figure 6. a) Cyclic voltammograms of **1**-(ClO$_4$)$_2$ and b) cyclic voltammograms (——) and differential pulse voltammograms (-----) of **2** in CH$_3$CN.

Table 4. Redox potentials of complexes.[a]

$n/n-1$[b]	Couple	$E_{1/2}$ (ΔE_{pp})[c]	Couple	$E_{1/2}$ (ΔE_{pp})[c]
6/5	–	–	$\mathbf{2}^{2+}/\mathbf{2}^+$	1.22 (110)
5/4	–	–	$\mathbf{2}^+/\mathbf{2}$	0.61 (80)
4/3	$\mathbf{1}^{4+}/\mathbf{1}^{3+}$	0.79 (95)	$\mathbf{2}/\mathbf{2}^-$	−0.48 (90)
3/2	$\mathbf{1}^{3+}/\mathbf{1}^{2+}$	0.27 (90)	$\mathbf{2}^-/\mathbf{2}^{2-}$	−1.18 (90)
2/1	$\mathbf{1}^{2+}/\mathbf{1}^+$	−1.02 (70)	–	–
1/0	$\mathbf{1}^+/\mathbf{1}$	−1.51 (80)	–	–
0/–	$\mathbf{1}/\mathbf{1}^-$[d]	−1.70 (60)	–	–

[a] From cyclic voltammetry in CH$_3$CN/0.1 M NEt$_4$ClO$_4$ at 100 mV s^{-1}. [b] Charge change of the [Ru(μ-H$_2$L)Ru]$^{(n/n-1)+}$ core. [c] In V versus SCE; peak potential differences ΔE_{pp} in mV (in parentheses). [d] Further bpy-based reductions at −1.91 (80) and −2.02 (60) V (mV).
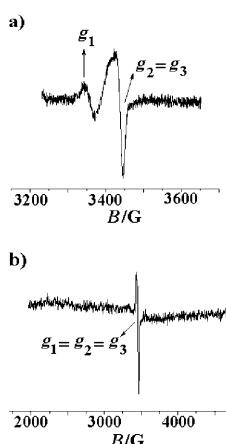
Figure 7. EPR spectra of a) 1^{3+} and b) 1^+ in $CH_3CN/0.1\,M$ Bu_4NPF_6 at 4 K.

in the near-infrared region (see later) and an axial EPR spectrum at 4 K (Figure 7a, Table 5). Both the small g anisotropy $g_1 - g_3 = 0.049$ and the average $g_{av} = 2.024$, close to the free-electron value of 2.0023, suggests a radical-complex[18] formulation $Ru^{II}(L^{•-})Ru^{II}$ for 1^{3+} instead of the mixed-valent alternative $Ru^{II}(L^{2-})Ru^{III}$.[19] The 520 mV separation between the oxidation couples in 1^{2+} leads to a comproportionation constant (K_c) of 6.5×10^8 for the paramagnetic intermediate (calculated using the equation $RT\ln K_c = nF(\Delta E)$), which

is significantly higher than the values observed for corresponding mixed-valent complexes of p-benzoquinone-derived bridging ligands such as $[\{(bpy)_2Ru\}_2(\mu\text{-}L^{2-})]^{2+}$, L^{2-} = 2,5-dioxido-1,4-benzoquinone ($K_c = 6 \times 10^5$),[4] 5,8-dioxido-1,4-naphthoquinone ($K_c = 1.8 \times 10^5$),[6] 1,4-dioxidoanthraquinone ($K_c = 3.7 \times 10^4$),[7] or 1,5-dioxidoanthraquinone ($K_c = 3.4 \times 10^2$).[7] A neutral 1,2,4,5-tetraimino-3,6-diketocyclohexane-bridged bis[Ru(bpy)$_2$] complex also showed a rather low K_c value at 10^5.[10] On the other hand, the diruthenium complex $[\{(NH_3)_5Ru\}_2(\mu\text{-}H_2L')]^{5+}$ involving the neutral bis-monodentate p-benzoquinonediimine bridging ligand (H_2L')[20] exhibits a K_c value of 10^{10}. The effects on K_c of strongly σ-donating NH_3 (and of $acac^-$) as ancillary ligands in comparison to π-acidic bpy were demonstrated earlier in a series of tetrazine-bridged diruthenium systems, $[(bpy)_2Ru(\mu\text{-}bptz)Ru(bpy)_2]^{5+}$ ($K_c = 10^{8.5}$),[21] $[(acac)_2Ru(\mu\text{-}bptz)Ru(acac)_2]^+$ ($K_c = 10^{13.6}$),[14b] and $[(NH_3)_4Ru(\mu\text{-}bptz)Ru(NH_3)_4]^{5+}$ ($K_c = 10^{15.0}$),[22] in which bptz = 3,6-bis(2-pyridyl)-1,2,4,5-tetrazine.

Complex $1\text{-}(ClO_4)_2$ exhibits multiple reduction processes in the range between −1 and −2 V versus SCE (Table 4). Stepwise reductions of the coordinated bridging ligand, $H_2L^{2-} \rightarrow H_2L^{•3-}$ and $H_2L^{•3-} \rightarrow H_2L^{4-}$, occur at −1.02 and −1.51 V, respectively, followed by successive bpy-based reduction processes (Table 4). The comproportionation con-

stant for the diruthenium complex 1^+ with the bridging radical trianion $H_2L^{•3-}$ is of a similar magnitude ($K_c = 2 \times 10^8$) to that of 1^{3+}. The intermediate 1^+ displays a free-radical-type EPR signal at $g = 1.995$, indicative of $\mu\text{-}H_2L^{•3-}$ bridging two Ru^{II} centers (see Figure 7b, Table 5).[23] No intense absorption was observed beyond 900 nm.

The complex $[\{(acac)_2Ru^{III}\}_2(\mu\text{-}H_2L^{2-})]$ (**2**) exhibits two successive one-electron couples on oxidation (Figure 6b, Table 4). The cyclic-voltammetric current associated with the second oxidation process appears larger than that involved with the other reversible processes, due to the onset of solvent oxidation; however, a direct comparison of differential pulse-voltammetric current heights relative to the other reversible processes establishes unequivocally two one-electron-transfer processes with a large K_c value of 2.1×10^{10} for the intermediate 2^+. That intermediate exhibits a rather intense near-infrared absorption (see later), but there was little change in the EPR signal except for some decrease in intensity (Table 5). The Ru^{III}-type EPR signal points to a $Ru^{III}(\mu\text{-}H_2L^{2-})Ru^{IV}$ formulation; however, it may also be possibly caused by contributions from an alternative formulation in which the bridging ligand is oxidized to yield a three-spin situation $Ru^{III}(\mu\text{-}H_2L^{•-})Ru^{III}$. The occurrence of a near-infrared band (see below) favors the former alternative in which an intervalence charge-transfer (IVCT) transition could be induced.

In addition, **2** also shows two successive one-electron reduction processes with a K_c value for the intermediate of 7.3×10^{11}, which could correspond either to successive Ru^{II}/Ru^{III} couples or to the bridging-ligand-based transitions $H_2L^{2-} \rightarrow H_2L^{•3-}$ and $H_2L^{•3-} \rightarrow H_2L^{4-}$. Considering the observed rhombic EPR spectrum of the one-electron-reduced intermediate 2^- at 4 K with $g_1 = 2.31$, $g_2 = 2.11$ and $g_3 = 1.90$ (Figure 8b, Table 5), it may be tempting to assume that the reduction occurs primarily at the metal ions although both formulations $Ru^{II}(\mu\text{-}H_2L^{2-})Ru^{III}$ and $Ru^{III}(\mu\text{-}H_2L^{•3-})Ru^{III}$ may produce metal-centered spin. The absence of near-infrared absorptions (see below) may indicate the latter alternative without a mixed-valence situation. The presence of electron-rich $acac^-$ functions in **2** reduces the Ru^{II}/Ru^{III} potential by ~0.8 V relative to the bpy derivative 1^{2+}, which leads to a preference for the ruthenium(III) state in **2** (Scheme 1).

Spectroelectrochemistry: Multiple intraligand transitions of 1^{2+} appear in the UV region (Table 6). In addition, two intense metal-to-ligand charge-transfer (MLCT) transitions with similar intensities are observed at 632 nm ($\varepsilon =$
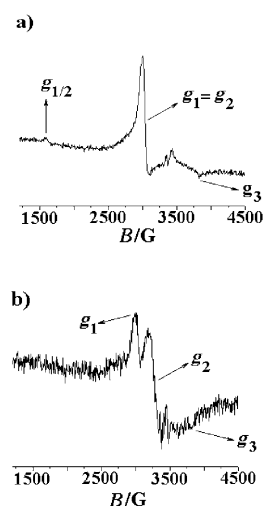
Table 5. EPR data[a] of paramagnetic states[b] and comproportionation constants K_c.

	G_1	g_2	g_3	g_{av}	$\Delta g = g_1 - g_3$	K_c[c]
1^{3+}	2.057	2.008	2.008	2.024	0.049	6.5×10^8
1^+	1.995	1.995	1.995	1.995	<0.01	2.0×10^8
2^+	2.26	2.26	1.81	2.11	0.45	2.2×10^{10}
2[d]	2.26	2.26	1.81	2.11	0.45	3.0×10^{18}
2^-	2.31	2.11	1.90	2.11	0.41	7.3×10^{11}

[a] g components measured at 4 K. [b] From EPR spectroelectrochemistry in $CH_3CN/0.1\,M$ Bu_4NPF_6, except for **2**. [c] Comproportionation constant from $RT\ln K_c = nF(\Delta E)$; for ΔE see Table 4. [d] Half-field signal at $g_{1/2} = 4.26$.

Figure 8. EPR spectra of a) **2** and b) 2^- in $CH_3CN/0.1\,M$ Bu_4NPF_6 at 4 K.

Table 6. UV-visible-NIR data of $\mathbf{1}^n$ [$n = 0, 1, 2, 3, 4$] and $\mathbf{2}^m$ [$m = -2, -1, 0, 1, 2$] from spectroelectrochemistry.[a]

	λ_{max} [nm] (ε [M^{-1}cm^{-1}])
$\mathbf{1}^{4+}$	1130(2720), 597(16 300), 465(6650), 375(sh), 315(sh), 295(25 800), 270(sh), 244(25 100)
$\mathbf{1}^{3+}$	1425(11 300), 705(17 900), 450(5750), 295(28 400), 280(sh), 240(26 200)
$\mathbf{1}^{2+}$	632(18 650), 550(18 500), 392(sh), 347(9500), 297(28 200), 280(sh), 242(25 000)
$\mathbf{1}^{+}$	840(5150), 613(12 100), 465(9400), 370(10 100), 296(28 200), 281(sh), 241(25 000)
$\mathbf{1}$	651(4000), 540(sh), 490(sh), 355(7850), 295(15 100), 240(13 500)
$\mathbf{2}^{2+}$	612(6000), 284(12 700)
$\mathbf{2}^{+}$	1565(4400), 698(14 300), 276(16 600), 240(sh)
$\mathbf{2}$	545(17 750), 340(sh), 280(20 700)
$\mathbf{2}^{-}$	735(32 200), 396(8950), 273(24 900)
$\mathbf{2}^{2-}$	855(27 600), 505(8100), 272(30 600)

[a] Measurements in CH$_3$CN/0.1 M Bu$_4$NPF$_6$ (OTTLE spectroelectrochemistry).

18 650 M^{-1}cm^{-1}) (Ru→H$_2$L^{2-}) and 550 nm (ε = 18 500 M^{-1}cm^{-1}) (Ru→bpy) (Figure 9a, Table 6). On oxidation to $\mathbf{1}^{3+}$, two new bands appear at 705 and 450 nm
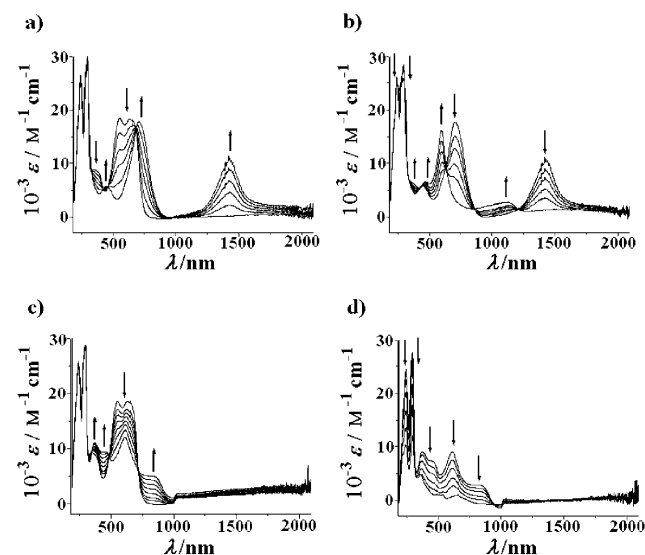

Figure 9. UV-visible-NIR spectroelectrochemistry for the conversions of a) $\mathbf{1}^{2+}$→$\mathbf{1}^{3+}$, b) $\mathbf{1}^{3+}$→$\mathbf{1}^{4+}$, c) $\mathbf{1}^{2+}$→$\mathbf{1}^{+}$, and d) $\mathbf{1}^{+}$→$\mathbf{1}$ in CH$_3$CN/0.1 M Bu$_4$NPF$_6$ (the step at 1000 nm is a detector switch artifact).

(MLCT or LMCT), along with a very intense near-infrared transition at 1425 nm (ε = 11 300 M^{-1}cm^{-1}) with a width-at-half-height ($\Delta\nu_{1/2}$) of 1000 cm^{-1}. The experimentally obtained $\Delta\nu_{1/2}$ value is much less than what would be calculated at 4026 cm^{-1} using the Hush formula [$\Delta\nu_{1/2} = (2310 E_{op})^{1/2}$][24] for a localized Class II mixed-valent system. This disagreement and the very high intensity of the absorption support the notion of a ligand-based oxidation to Ru^{II}(μ-H$_2$L$^{\cdot-}$)Ru^{II}, as strongly suggested by the EPR result. It may be noted that the corresponding dinuclear [Ru(bpy)$_2$]$^{n+}$ complex of the 2,5-dioxido-1,4-benzoquinone bridging

ligand failed to show any IVCT band up to 1800 nm.[4a] On further oxidation to the presumably isovalent Ru^{III}Ru^{III} complex $\mathbf{1}^{4+}$, the near-infrared band disappears and Ru^{III}-based ligand-to-metal charge-transfer (LMCT) transitions are observed at 597 and 465 nm (Figure 9b).

On one-electron reduction to $\mathbf{1}^{+}$, the Ru^{II}-based MLCT transitions are blue-shifted from 632 to 613 nm and from 550 to 465 nm with substantial reduction in intensity (Figure 9c). This is in accord with placement of one electron in the LUMO of H$_2$L^{2-} (which thus becomes the singly occupied molecular orbital, SOMO). The reduction of the coordinated bridging ligand results in a moderately intense low-energy band at 840 nm (ε = 5150 M^{-1}cm^{-1}), which probably corresponds to an internal SOMO→LUMO transition of (H$_2$L^{3-}). On further reduction to $\mathbf{1}$, the radical-anion-based transition at low-energy disappears and the d(Ru)→π*(bpy) MLCT transition is red-shifted to 651 nm (Figure 9d). This is consistent with the second reduction forming the (μ-H$_2$L^{4-}) ligand.[21]

The native Ru^{III}Ru^{III} species $\mathbf{2}$ exhibits an intense H$_2$L^{2-}→Ru^{III}-based LMCT transition at 545 nm (ε = 17 750 M^{-1}cm^{-1}), in addition to ligand-based transitions in the ultraviolet region (Figure 10a, Table 6). In the one-elec-
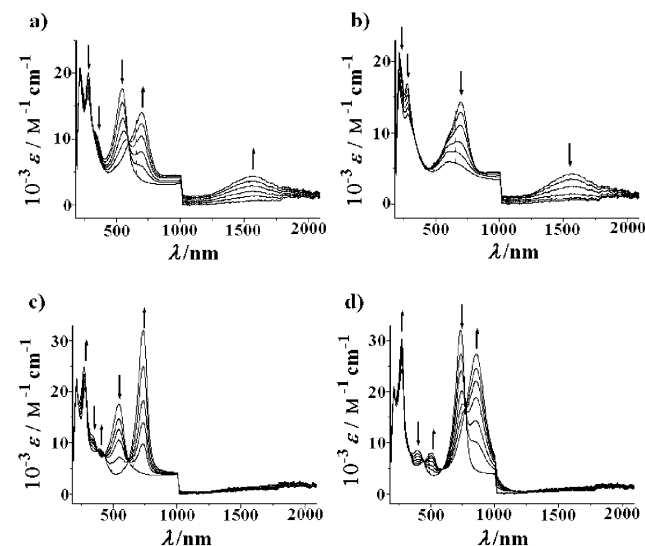

Figure 10. UV-visible-NIR spectroelectrochemistry for the conversions of a) $\mathbf{2}$→$\mathbf{2}^{+}$, b) $\mathbf{2}^{+}$→$\mathbf{2}^{2+}$, c) $\mathbf{2}$→$\mathbf{2}^{-}$, and d) $\mathbf{2}^{-}$→$\mathbf{2}^{2-}$ in CH$_3$CN/0.1 M Bu$_4$NPF$_6$ (the step at 1000 nm is an artifact from detector switching).

tron-oxidized species $\mathbf{2}^{+}$, the LMCT transition is red-shifted to 698 nm with a decrease in intensity, and a moderately intense IVCT band appears at 1565 nm (ε = 4400 M^{-1}cm^{-1}), in agreement with expectations for a mixed-valent Ru^{III}(μ-H$_2$L^{2-})Ru^{IV} species (Figure 10a). The width-at-half-height ($\Delta\nu_{1/2}$) of the IVCT band is measured at 2000 cm^{-1}, which is narrower than that obtained by means of the Hush theory (3842 cm^{-1}).[24] This implies a Class III mixed-valent state of $\mathbf{2}^{+}$, as is also suggested by the high K_c value of 2.1×10^{10}. Considering the Class III characteristics, V_{ab} is calculated as

$E_{op}/2$ at 3195 cm^{-1}.[25] On further one-electron oxidation to the Ru^{IV}Ru^{IV} state in **2**$^{2+}$, the IVCT band disappears and a moderately intense LMCT absorption appears at 612 nm (Figure 10b).

The one-electron-reduced form **2**$^-$ displays an unusually strong and narrow absorption band at 735 nm ($\varepsilon = 32200$ M^{-1}cm^{-1}) (Figure 10c). The species fails to show any distinct band in the near-infrared region. It should be noted that very weak-to-undetectable IVCT bands have been reported previously for the Ru^{II}Ru^{III} mixed-valent state for diruthenium– and triruthenium–acac systems[1a,e, 22, 26] in spite of reasonably large K_c values, and it was concluded that large K_c values are independent of the IVCT band intensity.[26b] However, **2**$^-$ displays a rhombic Ru^{III}-type EPR spectrum (Figure 8b). Assuming a Ru^{III}(μ-H$_2$L^{3-})Ru^{III} formulation with partially coupled spins because of the absent near-infrared absorption, we would have to assign the very intense band at 735 nm to a predominantly LMCT transition. Strong mixing of metal and ligand orbitals could explain the very narrow ($\Delta\nu_{1/2} = 1540$ cm^{-1}) and thus the intense band appearance. On further reduction to **2**$^{2-}$, this charge-transfer band is red-shifted to 855 nm with a slight decrease in intensity ($\varepsilon = 27600$ M^{-1}cm^{-1}) (Figure 10d). Both the Ru^{II}(μ-H$_2$L^{2-})Ru^{II} and Ru^{III}(μ-H$_2$L^{4-})Ru^{III} descriptions can be assumed.

The above observations are supported by the computed vertical excitation energies, using the time-dependent density functional theory (TD-DFT) method.[27] Sets of key transitions are given in Tables 7 and 8 in the text, and in Ta-
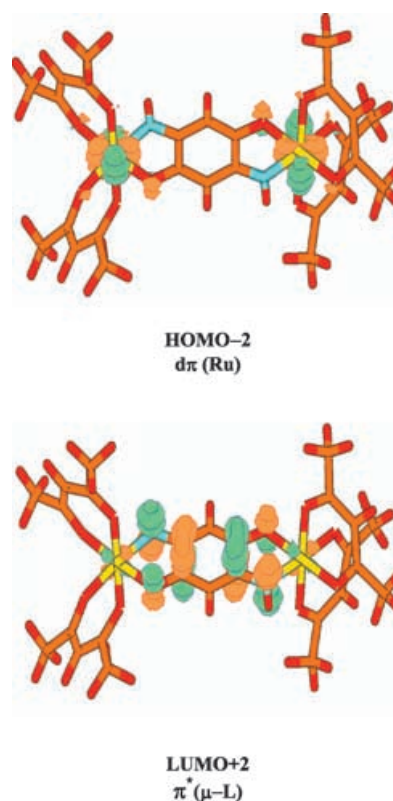

HOMO−2
dπ (Ru)

LUMO+2
π^*(μ−L)

Figure 11. Representative orbital contours for **2**.

In the case of complex **2**, the highest intensity charge-transfer transitions are predicted to be between dπ_{Ru} and π^*(μ-H$_2$L^{2-}). The low-energy transitions for **1**$^{2+}$ are found to be of a similar type, even though the donor orbital shows slight mixing with π(μ-H$_2$L^{2-}). The experimentally observed UV-visible transitions for both **2** and **1**$^{2+}$ are in reasonable agreement with the computed values. For instance, the MLCT band for **2** appearing at 545 nm ($\varepsilon = 17750$ M^{-1}cm^{-1}) is in agreement with the computed value at 504 nm ($\varepsilon = 23814$ M^{-1}cm^{-1}). Similarly, for complex **1**$^{2+}$ the MLCT transition of 632 nm ($\varepsilon = 18650$ M^{-1}cm^{-1}) is comparable to the calculated value of 638 nm ($\varepsilon = 13238$ M^{-1}cm^{-1}). The predicted low-energy transitions for **2** (HOMO→LUMO, HOMO−1→LUMO+1) are of zero oscillator strength and are not observed experimentally.

Table 7. Selected list of higher intensity vertical excitations computed at the TD-DFT/B3LYP//B3LYP/3–21G level[a] for **1**$^{2+}$.

Excitation energy[a,b]	Oscillator strength	ε[c]	$\psi_o-\psi_v$[d]	Type of transition
15668 (638)	0.1885	13238	HOMO→LUMO (0.61)[e]	dπ(Ru), π(μ-H$_2$L^{2-})→π^*(μ-H$_2$L^{2-})
16640 (601)	0.0156	1096	HOMO→LUMO+2 (0.51)	dπ(Ru), π(μ-H$_2$L^{2-})→π^*(bipy), dπ(Ru)
17122 (584)	0.0409	2872	HOMO−1→LUMO+3 (0.55)	dπ(Ru), π(μ-H$_2$L^{2-})→π^*(bipy)

[a] Calculations were done by employing a LanL2DZ basis set for Ru and 3–21G for the other elements; singlet excitation energies in cm^{-1}. [b] Wavelengths in nm given in parentheses. [c] ε in M^{-1}cm^{-1}. [d] Occupied and virtual orbitals. [e] Transition coefficients.

Table 8. Selected list of vertical excitations computed at the TD-DFT/B3LYP//B3LYP/3–21G level[a] for **2**.

Excitation energy[a,b]	Oscillator strength	ε[c]	$\psi_o-\psi_v$[d]	Type of transition
2770 (3610)	0.0000	0.00	HOMO→LUMO (0.90)[e]	dπ(Ru), π(acac)→dπ(Ru)
17710 (565)	0.0000	0.00	HOMO−1→LUMO+1 (0.77)	dπ(Ru), π(μ-H$_2$L^{2-})→dπ(Ru)
19830 (504)	0.3391	23814	HOMO−2→LUMO+2 (0.73)	dπ(Ru)→π^*(μ-H$_2$L^{2-})
20000 (500)	0.5065	35570	HOMO−2→LUMO+2 (0.59)	dπ(Ru)→π^*(μ-H$_2$L^{2-})

[a] Calculations were done by employing LanL2DZ basis set for Ru and 3–21G for other elements; triplet excitation energies in cm^{-1}. [b] Wavelengths in nm given in parentheses. [c] ε in M^{-1}cm^{-1}. [d] Occupied and virtual orbitals. [e] Transition coefficients.

bles S7 and S8 in the Supporting Information, representative orbital contours are shown in Figure 11. Other orbital contours for **2** and **1**$^{2+}$ are provided in the Supporting Information (Tables S2 and S3).

It is interesting to note that the higher-energy transitions predicted for 1^{2+} are of an MLCT-type involving π^*(bpy) as the acceptor (see Table 7 and Table S8 in the Supporting Information). For instance, the transition at 584 nm corresponds to HOMO$-1\rightarrow$LUMO$+3$. While there are minor contributions (mixing) to $d\pi_{Ru}$ (HOMO-1) from the bridging ligand orbitals, the LUMO$+3$ is mostly located on bpy. A complete list of various other computed transitions is provided in Table S8 in the Supporting Information. The nature of these transitions is identified by using the orbital contours as shown in Table S3 in the Supporting Information. The computed HOMO–LUMO energy gap for **2** is found to be lower than that of 1^{2+} by 0.48 eV (Table S6 in the Supporting Information).

The presence of Ru^{III} centers in **2** is further supported by the computed spin densities on both Ru centers which amounts to 0.81, clearly indicating the presence of one unpaired electron on each metal center.

Conclusion

Starting from the unequivocally established compounds $[(bpy)_2Ru^{II}(\mu\text{-}H_2L^{2-})Ru^{II}(bpy)_2](ClO_4)_2$ (**1**-(ClO$_4$)$_2$) and $[(acac)_2Ru^{III}(\mu\text{-}H_2L^{2-})Ru^{III}(acac)_2]$ (**2**) with the previously unexploited 2,5-dioxido-1,4-benzoquinonediimine bridging ligand H_2L^{2-} we have attempted to establish the oxidation state distribution for various accessible redox states of these compounds, using a combination of UV-visible-NIR and EPR spectroelectrochemistry. The results are summarized in Scheme 2.
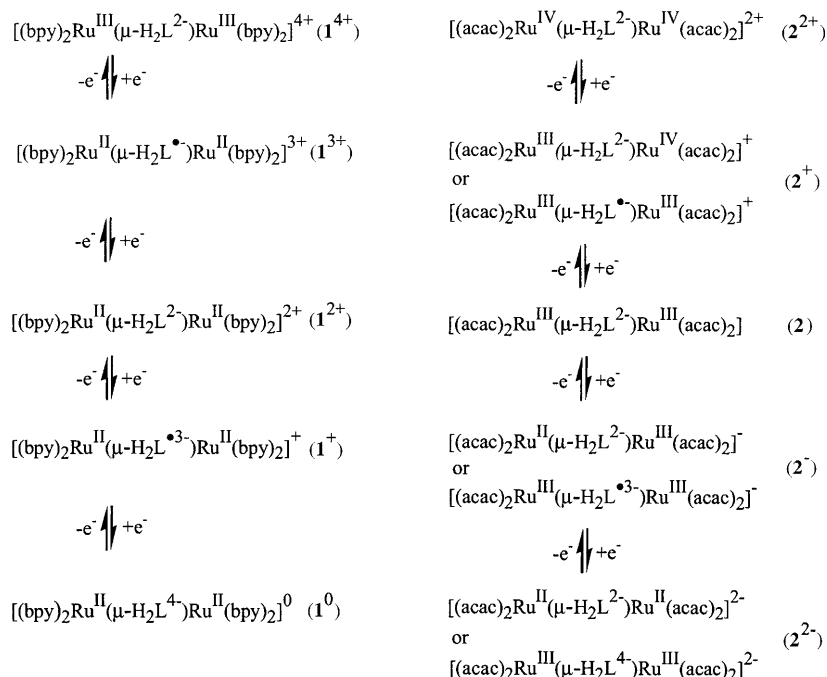
Scheme 2 illustrates that the dinuclear complexes 1^{n+} prefer the bis(2,2′-bipyridine)ruthenium(II) configuration. Electron-transfer occurs largely at the bridging ligand $\mu\text{-}H_2L^{n-}$ as evident from radical ($\mu\text{-}H_2L^{\cdot-}$ or $\mu\text{-}H_2L^{\cdot3-}$) EPR signals for 1^{3+} and 1^+. In contrast, higher metal oxidation states (Ru^{III}, Ru^{IV}) seem to be favored by the dinuclear bis(acetylacetonato)ruthenium complexes 2^m, leading to more complex and ambivalent oxidation state combinations. Intense long-wavelength absorption bands and Ru^{III}-type EPR signals point to mixed-valent dimetal configurations of the intermediates 2^+ and 2^-; however, three-spin arrangements with two ruthenium(III) centers and radical ligand bridges $\mu\text{-}H_2L^{\cdot-}$ or $\mu\text{-}H_2L^{\cdot3-}$ cannot be ruled out. The results confirm again the essential role of ancillary ligands in determining oxidation state distributions within potential redox-ambivalent arrangements between electro-active metal ions and organic mediators. Clearly, H_2L^{2-} is a good noninnocent[3g,h] bis-chelating ligand, a hitherto neglected member of the quinone ligand family. An additional feature emerging from the study of this particular ligand is the potential for interligand and ligand–solvent hydrogen bonding, which could eventually lead to a better understanding of metal–ligand electron-transfer control through hydrogen-bonded networks, as is typical for many metalloproteins.[14]

Experimental Section

$[(bpy)_2Ru^{III}(\mu\text{-}H_2L^{2-})Ru^{III}(bpy)_2]^{4+}$ (1^{4+})

$-e^-\ \Updownarrow\ +e^-$

$[(bpy)_2Ru^{II}(\mu\text{-}H_2L^{\cdot-})Ru^{II}(bpy)_2]^{3+}$ (1^{3+})

$-e^-\ \Updownarrow\ +e^-$

$[(bpy)_2Ru^{II}(\mu\text{-}H_2L^{2-})Ru^{II}(bpy)_2]^{2+}$ (1^{2+})

$-e^-\ \Updownarrow\ +e^-$

$[(bpy)_2Ru^{II}(\mu\text{-}H_2L^{\cdot3-})Ru^{II}(bpy)_2]^{+}$ (1^{+})

$-e^-\ \Updownarrow\ +e^-$

$[(bpy)_2Ru^{II}(\mu\text{-}H_2L^{4-})Ru^{II}(bpy)_2]^{0}$ (1^{0})

$[(acac)_2Ru^{IV}(\mu\text{-}H_2L^{2-})Ru^{IV}(acac)_2]^{2+}$ (2^{2+})

$-e^-\ \Updownarrow\ +e^-$

$[(acac)_2Ru^{III}(\mu\text{-}H_2L^{2-})Ru^{IV}(acac)_2]^{+}$
or
$[(acac)_2Ru^{III}(\mu\text{-}H_2L^{\cdot-})Ru^{III}(acac)_2]^{+}$ (2^{+})

$-e^-\ \Updownarrow\ +e^-$

$[(acac)_2Ru^{III}(\mu\text{-}H_2L^{2-})Ru^{III}(acac)_2]$ (2)

$-e^-\ \Updownarrow\ +e^-$

$[(acac)_2Ru^{II}(\mu\text{-}H_2L^{2-})Ru^{III}(acac)_2]^{-}$
or
$[(acac)_2Ru^{III}(\mu\text{-}H_2L^{\cdot3-})Ru^{III}(acac)_2]^{-}$ (2^{-})

$-e^-\ \Updownarrow\ +e^-$

$[(acac)_2Ru^{II}(\mu\text{-}H_2L^{2-})Ru^{II}(acac)_2]^{2-}$
or
$[(acac)_2Ru^{III}(\mu\text{-}H_2L^{4-})Ru^{III}(acac)_2]^{2-}$ (2^{2-})

Scheme 2.

(SCE) were used in a three-electrode configuration. The supporting electrolyte was [NEt$_4$]ClO$_4$ (0.1 M) and the solute concentration was ~10^{-3} M. The half-wave potential E^o_{298} was set equal to $0.5(E_{pa}+E_{pc})$, in which E_{pa} and E_{pc} are the anodic and cathodic cyclic-voltammetric peak potentials, respectively. A platinum wire-gauze working electrode was used in the coulometric experiments. The elemental analyses were carried out with a Perkin–Elmer 240C elemental analyzer. Electrospray mass spectra were recorded on a Micromass Q-ToF mass spectrometer. The magnetic susceptibility of **1**-(ClO$_4$)$_2$ and **2** as a function of temperature was recorded from 1.8 to 300 K by using a 0.1 T applied field on a Quantum Design MPMS XL7 SQUID magnetometer. The data were corrected for diamagnetic contributions to the magnetic susceptibility by using Pascal's constants and for the diamagnetic contribution from the sample holder.

Caution! Perchlorate salts of metal complexes with organic ligands are potentially explosive. Heating of dried samples must be avoided; handling of small amounts must proceed with great caution using protection.

[{(bpy)$_2$Ru}$_2$(H$_2$L)](ClO$_4$)$_2$ (1-(ClO$_4$)$_2$): The starting complex *cis*-[Ru-(bpy)$_2$Cl$_2$]·2H$_2$O (100 mg, 0.20 mmol) and AgClO$_4$ (108.6 mg, 0.52 mmol) were added to absolute ethanol (15 mL), and the mixture was refluxed for 2 h with stirring. The initial violet solution changed to orange-red; the mixture was then cooled and filtered through a sintered glass funnel. The ligand H$_6$L (21 mg, 0.10 mmol) was added to the above solution containing [Ru(bpy)$_2$(EtOH)$_2$]$^{2+}$, followed by sodium acetate (34 mg, 0.40 mmol). The resulting mixture was heated under reflux for 12 h under a dinitrogen atmosphere. The resultant solution was reduced to 5 mL and kept at 0°C overnight. The blue precipitate that formed on cooling was filtered and washed thoroughly with ice-cold water followed by cold ethanol and diethyl ether. The product was recrystallized from acetonitrile/benzene (1:4). Yield: (70 mg, 63%); elemental analysis calcd (%) for Ru$_2$C$_{46}$H$_{36}$N$_{10}$O$_{10}$Cl$_2$ (1161.90): C 47.55, H 3.12, N 12.06; found: C 47.73, H 3.46, N 12.36; Λ_M in acetonitrile at 25°C: 230 Ω^{-1} cm^2 M^{-1}.

[{(acac)$_2$Ru}$_2$(H$_2$L)] (2): The starting complex [Ru(acac)$_2$(CH$_3$CN)$_2$] (100 mg, 0.26 mmol), the ligand H$_6$L (28 mg, 0.13 mmol) and sodium acetate (44 mg, 0.52 mmol) were dissolved in ethanol (20 mL) and the mixture was heated under reflux for 12 h under a dinitrogen atmosphere. The initial orange solution gradually changed to purple-red. The solvent of the reaction mixture was evaporated to dryness under reduced pressure and the residue was then purified using a neutral alumina column. Initially, a red compound corresponding to [Ru(acac)$_3$] was eluted by CH$_2$Cl$_2$/CH$_3$CN (25:1), followed by a purple-red compound with CH$_2$Cl$_2$/CH$_3$CN (10:1), corresponding to **2**. Evaporation of solvent under reduced pressure yielded the pure complex **2**. Yield: (45 mg, 47%); elemental analysis calcd (%) for Ru$_2$C$_{26}$H$_{32}$N$_2$O$_{10}$ (734.69): C 42.51, H 4.39, N 3.81; found: C 42.72, H, 4.67, N 3.98.

Crystallography: Single crystals of **2**·2H$_2$O were grown by slow diffusion of a solution of the complex in undried acetonitrile into benzene, followed by slow evaporation under atmospheric conditions. The crystal data of **2**·2H$_2$O were collected on a Bruker SMART APEX CCD diffractometer at 293 K. Selected data collection parameters and other crystallographic results are summarized in Table 1. All data were corrected for Lorentz polarization and absorption effects. The program package SHELX-97 (SHELXTL)[31,32] was used for structure solution and full-matrix least-squares refinement on F^2. Hydrogen atoms were included in the refinement using the riding model. Contributions of hydrogen atoms for the water molecules were included but were not fixed.

CCDC-264905 contains the supplementary crystallographic data for **2**. These data can be obtained free of charge via www.ccdc.cam.ac.uk/data_request/cif.

Computational details: Complete geometry optimization was carried out using the density functional theory method at the (U)B3LYP level. All elements except ruthenium were assigned 3–21G basis set. A Los Alamos effective core potential (ECP) with a double zeta quality (DZ) valence basis set (LanL2DZ) was employed for the ruthenium atoms.[33a–c] Calculations were performed with Gaussian98.[33d] Vertical electronic excitations based on B3LYP-optimized geometries were computed by using the time-dependent density functional theory (TD-DFT) formalism[33e,f] with the B3LYP functional with the above combination of basis sets. Visual inspection of all key orbitals was done with MOLDEN[33g] to assign the nature of various electronic transitions.

[1] a) S. Patra, B. Sarkar, S. Ghumaan, J. Fiedler, W. Kaim, G. K. Lahiri, *Inorg. Chem.* **2004**, *43*, 6108; b) N. Chanda, B. Sarkar, S. Kar, J. Fiedler, W. Kaim, G. K. Lahiri, *Inorg. Chem.* **2004**, *43*, 5128; c) S. Kar, N. Chanda, S. M. Mobin, A. Datta, F. A. Urbanos, V. G. Puranik, R. Jimenez -Aparicio, G. K. Lahiri, *Inorg. Chem.* **2004**, *43*, 4911; d) S. Kar, B. Pradhan, R. K. Sinha, T. Kundu, P. Kodgire, K. K. Rao, V. G. Puranik, G. K. Lahiri, *Dalton Trans.* **2004**, 1752; e) S. Patra, B. Sarkar, S. Ghumaan, J. Fiedler, W. Kaim, G. K. Lahiri, *Dalton Trans.* **2004**, 754; f) S. Patra, B. Sarkar, S. Ghumaan, J. Fiedler, S. Zalis, W. Kaim, G. K. Lahiri, *Dalton Trans.* **2004**, 750; g) B. Sarkar, W. Kaim, A. Klein, B. Schwederski, J. Fiedler, C. Duboc-Toia, G. K. Lahiri, *Inorg. Chem.* **2003**, *42*, 6172; h) S. Patra, T. A. Miller, B. Sarkar, M. Niemeyer, M. D. Ward, G. K. Lahiri, *Inorg. Chem.* **2003**, *42*, 4707; i) N. Chanda, B. Sarkar, J. Fiedler, W. Kaim, G. K. Lahiri, *Dalton Trans.* **2003**, 3550; j) S. Kar, T. A. Miller, S. Chakraborty, B. Sarkar, B. Pradhan, R. K. Sinha, T. Kundu, M. D. Ward, G. K. Lahiri, *Dalton Trans.* **2003**, 2591; k) S. Patra, B. Mondal, B. Sarkar, M. Niemeyer, G. K. Lahiri, *Inorg. Chem.* **2003**, *42*, 1322; l) N. Chanda, R. H. Laye, S. Chakraborty, R. L. Paul, J. C. Jeffery, M. D. Ward, G. K. Lahiri, *J. Chem. Soc. Dalton Trans.* **2002**, 3496; m) S. Chakraborty, R. H. Laye, P. Munshi, R. L. Paul, M. D. Ward, G. K. Lahiri, *J. Chem. Soc. Dalton Trans.* **2002**, 2348; n) B. Sarkar, R. H. Laye, B. Mondal, S. Chakraborty, R. L. Paul, J. C. Jeffery, V. G. Puranik, M. D. Ward, G. K. Lahiri, *J. Chem. Soc. Dalton Trans.* **2002**, 2097; o) S. Chakraborty, R. H. Laye, R. L. Paul, R. G. Gonnade, V. G. Puranik, M. D. Ward, G. K. Lahiri, *J. Chem. Soc. Dalton Trans.* **2002**, 1172.

[2] a) F. Paul, C. Lapinte, *Coord. Chem. Rev.* **1998**, *178–180*, 431; b) M. D. Ward, *Chem. Ind.* **1997**, 640; c) M. D. Ward, *Chem. Ind.* **1996**, 568.

[3] a) S. Patra, B. Sarkar, S. M. Mobin, W. Kaim, G. K. Lahiri, *Inorg. Chem.* **2003**, *42*, 6469; b) P. Ghosh, A. Begum, D. Herebian, E. Bothe, K. Hildenbrand, T. Weyhermüller, K. Wieghardt, *Angew. Chem.* **2003**, *115*, 581; *Angew. Chem. Int. Ed.* **2003**, *42*, 563; c) K. S. Min, T. Weyhermüller, K. Wieghardt, *Dalton Trans.* **2003**, 1126; d) S. Bhattacharya, P. Gupta, F. Basuli, C. G. Pierpont, *Inorg. Chem.* **2002**, *41*, 5810; e) H. Chun, E. Bill, E. Bothe, T. Weyhermüller, K. Wieghardt, *Inorg. Chem.* **2002**, *41*, 5091; f) W. Kaim, M. Wanner, A. Knödler, S. Zalis, *Inorg. Chim. Acta* **2002**, *337*, 163; g) C. G. Pierpont, *Coord. Chem. Rev.* **2001**, *219–221*, 415; h) P. Chaudhuri, C. N. Verani, E. Bill, E. Bothe, T. Weyhermüller, K. Wieghardt, *J. Am. Chem. Soc.* **2001**, *123*, 2213; i) C. G. Pierpont, A. S. Attia, *Collect. Czech. Chem. Commun.* **2001**, *66*, 33; j) J. Rall, M. Wanner, M. Albrecht, F. M. Hornung, W. Kaim, *Chem. Eur. J.* **1999**, *5*, 2802; k) C. N. Verani, S. Gallert, E. Bill, T. Weyhermüller, K. Wieghardt, P. Chaudhuri, *Chem. Commun.* **1999**, 1747; l) M. Ebadi, A. B. P. Lever, *Inorg. Chem.* **1999**, *38*, 467; m) J. Rall, E. Waldhör, B. Schwederski, M. Schwach, S. Kohlmann, W. Kaim, in *Bioinorganic Chemistry: Transition Metals in Biology and their Coordination Chemistry* (Ed.: A. X. Trautwein), VCH, Weinheim, **1997**, p. 476; n) R. A. Metcalfe, A. B. P. Lever, *Inorg. Chem.* **1997**, *36*, 4762; o) G. Speier, A. Whalen, J. Csihony, C. G. Pierpont, *Inorg. Chem.* **1995**, *34*, 1355; p) C. G. Pierpont, C. W. Lange, *Prog. Inorg. Chem.* **1994**, *41*, 331; q) J. Rall, W. Kaim, *J. Chem. Soc. Faraday Trans.* **1994**, *90*, 2905; r) H. Masui, A. B. P. Lever, E. S. Dodsworth, *Inorg. Chem.* **1993**, *32*, 258; s) B. Schwederski, W. Kaim, *Inorg. Chim. Acta* **1992**, *195*, 123; t) N. Bag, G. K. Lahiri, P. Basu, A. Chakravorty, *J. Chem.*

Soc. Dalton Trans. **1992**, 113; u) N. Bag, A. Pramanik, G. K. Lahiri, *Inorg. Chem.* **1992**, *31*, 40; v) H. Masui, A. B. P. Lever, P. Auburn, *Inorg. Chem.* **1991**, *30*, 2402; w) A. Dei, D. Gatteschi, L. Pardi, *Inorg. Chem.* **1990**, *29*, 1443; x) S. Ernst, P. Hänel, J. Jordanov, W. Kaim, V. Kasack, E. Roth, *J. Am. Chem. Soc.* **1989**, *111*, 1733; y) S. Ernst, V. Kasack, C. Bessenbacher, W. Kaim, *Z. Naturforsch. B* **1987**, *42*, 425; z) M. Haga, E. S Dodsworth, A. B. P. Lever, *Inorg. Chem.* **1986**, *25*, 447; aa) R. B. Salmonsen, A. Abelleira, M. J. Clarke, *Inorg. Chem.* **1984**, *23*, 387; ab) A. Dei, D. Gatteschi, C. Sangregorio, L. Sorace, *Acc. Chem. Res.* **2004**, *37*, 827.

[4] a) M. D. Ward, *Inorg. Chem.* **1996**, *35*, 1712; b) A. Dei, D. Gatteschi, L. Pardi, U. Russo, *Inorg. Chem.* **1991**, *30*, 2589.

[5] a) H. Adams, X. Chen, B. E. Mann, *J. Chem. Soc. Dalton Trans.* **1996**, 2159; b) A. Elduque, Y. Garces, L. A. Oro, M. T. Pinillos, A. Tiripicchio, F. Ugozzoli, *J. Chem. Soc. Dalton Trans.* **1996**, 2155; c) C. Fujii, M. Mitsumi, M. Kodera, K.-I. Motoda, M. Ohba, N. Matsumoto, H. Okawa, *Polyhedron* **1994**, *13*, 933; d) M. A. Calvo, A. M. M. Lanfredi, L. A. Oro, M. T. Pinillos, C. Tejel, A. Tiripicchio, F. Ugozzoli, *Inorg. Chem.* **1993**, *32*, 1147; e) K. Lu, J. E. Earley, *Inorg. Chem.* **1993**, *32*, 189; f) S. Liu, S. N. Shaikh, J. Zubieta, *J. Chem. Soc. Chem. Commun.* **1988**, 1017; g) C. G. Pierpont, L. C. Francesconi, D. N. Hendrickson, *Inorg. Chem.* **1977**, *16*, 2367; h) C. G. Pierpont, H. H. Downs, *J. Am. Chem. Soc.* **1975**, *97*, 2123.

[6] A. Dei, D. Gatteschi, L. Pardi, *Inorg. Chem.* **1990**, *29*, 1442.

[7] G. G. Sadler, N. R. Gordon, *Inorg. Chim. Acta* **1991**, *180*, 271.

[8] a) J. Rall, A. F. Stange, K. Hubler, W. Kaim, *Angew. Chem.* **1998**, *110*, 2827; *Angew. Chem. Int. Ed.* **1998**, *37*, 2681; b) S. Frantz, J. Rall, I. Hartenbach, T. Schleid, S. Zalis, W. Kaim, *Chem. Eur. J.* **2004**, *10*, 149.

[9] a) O. Siri, P. Braunstein, *Chem. Commun.* **2000**, 2223; b) O. Siri, P. Braunstein, M. M. Rohmer, M. Bénard, R. Welter, *J. Am. Chem. Soc.* **2003**, *125*, 13793; c) M. Elhabiri, O. Siri, A. Sornosa-Tent, A.-M. Albrecht-Gary, P. Braunstein, *Chem. Eur. J.* **2004**, *10*, 134; d) P. Braunstein, A. Demessence, O. Siri, J.-P. Taquet, *C. R. Chim.* **2004**, *7*, 909.

[10] H. Masui, A. L. Freda, M. C. Zerner, A. B. P. Lever, *Inorg. Chem.* **2000**, *39*, 141.

[11] a) D. Zhang, G.-X. Jin, *Organometallics* **2003**, *22*, 2851; b) J.-P. Taquet, O. Siri, P. Braunstein, R. Welter, *Inorg. Chem.* **2004**, *43*, 6944.

[12] a) W. Kaim, *Dalton Trans.* **2003**, 761; b) J. E. Dove, J. P. Klinman, *Adv. Protein Chem.* **2001**, *58*, 141; c) M. Mure, S. A. Mills, J. P. Klinman, *Biochemistry* **2002**, *41*, 9269; d) M. R. Parsons, M. A. Convery, C. M. Wilmot, K. D. S. Vadav, V. Blakeley, A. S. Corner, S. E. V. Phillips, M. J. McPherson, P. F. Knowles, *Structure* **1995**, *3*, 1171; e) V. Kumar, D. M. Dooley, H. C. Freeman, J. M. Guss, I. Harvey, M. A. McGuirl, M. C. J. Wilce, V. M. Zubak, *Structure* **1996**, *4*, 943; f) R. Li, J. P. Klinman, F. S. Mathews, *Structure* **1998**, *6*, 293; g) C. M. Wilmot, J. Hajdu, M. J. McPherson, P. F. Knowles, S. E. V. Phillips, *Science* **1999**, *286*, 1724; h) D. M. Dooley, R. A. Scott, P. F. Knowles, C. M. Colangelo, M. A. McGuirl, D. E. Brown, *J. Am. Chem. Soc.* **1998**, *120*, 2599.

[13] a) S. K. Ghosh, P. K. Bharadwaj, *Inorg. Chem.* **2004**, *43*, 6887; b) S. K. Ghosh, P. K. Bharadwaj, *Angew. Chem.* **2004**, *116*, 3661; *Angew. Chem. Int. Ed.* **2004**, *43*, 3577; c) S. K. Ghosh, P. K. Bharadwaj, *Inorg. Chem.* **2004**, *43*, 5180; d) S. Neogi, G. Savitha, P. K. Bharadwaj, *Inorg. Chem.* **2004**, *43*, 3771; e) S. K. Ghosh, P. K. Bharadwaj, *Inorg. Chem.* **2003**, *42*, 8250; f) R. Ludwig, *Angew. Chem.* **2001**, *113*, 1856; *Angew. Chem. Int. Ed.* **2001**, *40*, 1808.

[14] a) *Water and Biological Macromolecules* (Ed.: E. Westhoff), CRC, Boca Raton FL, **1993**; b) *Handbook on Metalloproteins* (Eds.: I. Bertini, A. Sigel, H. Sigel), Marcel Dekker, New York, **2001**; c) W. Kaim, B. Schwederski, in *Bioinorganic Chemistry*, Wiley, Chichester, **1994**.

[15] a) S. Ernst, V. Kasack, W. Kaim, *Inorg. Chem.* **1988**, *27*, 1146; b) S. Chellamma, M. Lieberman, *Inorg. Chem.* **2001**, *40*, 3177.

[16] a) R. S. Drago, *Physical Methods for Chemists*, 2nd ed., Saunders College Publishing, New York, **1992**, p. 390; b) O. Kahn, *Molecular Magnetism*, VCH, New York, **1993**.

[17] a) S. Ghumaan, B. Sarkar, S. Patra, J. v. Slageren, J. Fiedler, W. Kaim, G. K. Lahiri, *Dalton Trans.* **2005**, 706; b) T. Tanase, Y. Yamada, K. Tanaka, T. Miyazu, M. Kato, K. Lee, Y. Sugihara, W. Mori, A. Ichimura, I. Kinoshita, Y. Yamamoto, M. Haga, Y. Sasaki, S. Yano, *Inorg. Chem.* **1996**, *35*, 6230.

[18] W. Kaim, *Coord. Chem. Rev.* **1987**, *76*, 187.

[19] V. Kasack, W. Kaim, H. Binder, J. Jordanov, E. Roth, *Inorg. Chem.* **1995**, *34*, 1924.

[20] S. Joss, H. Reust, A. Ludi, *J. Am. Chem. Soc.* **1981**, *103*, 981.

[21] a) S. D. Ernst, W. Kaim, *Inorg. Chem.* **1989**, *28*, 1520; b) K. C. Gordon, A. K. Burrell, T. J. Simpson, S. E. Page, G. Kelso, M. I. J. Polson, A. Flood, *Eur. J. Inorg. Chem.* **2002**, 554.

[22] J. Poppe, M. Moscherosch, W. Kaim, *Inorg. Chem.* **1993**, *32*, 2640.

[23] E. Waldhör, B. Schwederski, W. Kaim, *J. Chem. Soc. Perkin Trans. 2* **1993**, 2109.

[24] N. S. Hush, *Prog. Inorg. Chem.* **1967**, *8*, 391.

[25] D. Astruc, *Acc. Chem. Res.* **1997**, *30*, 383.

[26] a) B. D. Yeomans, L. S. Kelso, P. A. Tregloan, F. R. Keene, *Eur. J. Inorg. Chem.* **2001**, 239; b) W. Kaim, A. Klein, M. Glöckle, *Acc. Chem. Res.* **2000**, *33*, 755.

[27] a) R. Bauernschmitt, R. Alrichs, *Chem. Phys. Lett.* **1996**, *256*, 454; b) M. Casida, K. C. Jamorski, K. C. Casida, D. R. Salahub, *J. Chem. Phys.* **1998**, *108*, 4439; c) A. D. Becke, *Phys. Rev. A* **1988**, *38*, 3098; d) T. Matsubara, K. Hirao, *Organometallics* **2001**, *20*, 5759; e) I. Iwakura, H. Tanaka, T. Ikeno, T. Yamada, *Chem. Lett.* **2004**, *33*, 140; f) K. Zheng, J. Wang, W. Peng, X. Liu, F. Yun, *J. Phys. Chem. A* **2001**, *105*, 10899; g) J. M. Villegas, S. R. Stoyanov, W. Huang, L. L. Lockyear, J. H. Reibenspies, D. P. Rillema, *Inorg. Chem.* **2004**, *43*, 6383.

[28] a) T. Kobayashi, Y. Nishina, K. G. Shimizu, G. P. Satô, *Chem. Lett.* **1988**, 1137; b) B. P. Sullivan, D. J. Salmon, T. J. Meyer, *Inorg. Chem.* **1978**, *17*, 3334.

[29] M. Krejcik, M. Danek, F. Hartl, *J. Electroanal. Chem. Interfacial Electrochem* **1991**, *317*, 179.

[30] W. Kaim, S. Ernst, V. Kasack, *J. Am. Chem. Soc.* **1990**, *112*, 173.

[31] SHELXTL PC 5.03, Siemens Analytical X-ray Instruments Inc, Madison, WI, 1994.

[32] G. M. Sheldrick, SHELXS-97, Program for Crystal Structure Solution and Refinement, University of Göttingen, Göttingen (Germany), **1997**.

[33] a) P. J. Hay, W. R. Wadt, *J. Chem. Phys.* **1985**, *82*, 270; b) P. J. Hay, W. R. Wadt, *J. Chem. Phys.* **1985**, *82*, 299; c) W. R. Wadt, P. J. Hay, *J. Chem. Phys.* **1985**, *82*, 284; d) Gaussian 98 (Revision A.11.4), M. J. Frisch, G. W. Trucks, H. B. Schlegel, G. E. Scuseria, M. A. Robb, J. R. Cheeseman, V. G. Zakrzewski, J. A. Montgomery, Jr., R. E. Stratmann, J. C. Burant, S. Dapprich, J. M. Millam, A. D. Daniels, K. N. Kudin, M. C. Strain, O. Farkas, J. Tomasi, V. Barone, M. Cossi, R. Cammi, B. Mennucci, C. Pomelli, C. Adamo, S. Clifford, J. Ochterski, G. A. Petersson, P. Y. Ayala, Q. Cui, K. Morokuma, P. Salvador, J. J. Dannenberg, D. K. Malick, A. D. Rabuck, K. Raghavachari, J. B. Foresman, J. Cioslowski, J. V. Ortiz, A. G. Baboul, B. B. Stefanov, G. Liu, A. Liashenko, P. Piskorz, I. Komaromi, R. Gomperts, R. L. Martin, D. J. Fox, T. Keith, M. A. Al-Laham, C. Y. Peng, A. Nanayakkara, M. Challacombe, P. M. W. Gill, B. Johnson, W. Chen, M. W. Wong, J. L. Andres, C. Gonzalez, M. Head-Gordon, E. S. Replogle, J. A. Pople, Gaussian, Inc., Pittsburgh, PA, **2002**; e) C. Lee, W. Yang, R. G. Parr, *Phys. Rev. B* **1988**, *37*, 785; f) M. Casida in *Recent Advances in Density Functional Methods* (Ed.: D. P. Chong), World Scientific Press, Singapore, **1995**, Vol. I, pp. 155; g) G. Schaftenaar, J. H. Noordik, *J. Comput.-Aided Mol. Design* **2000**, *14*, 123.